49th AIAA Aerospace Sciences Meeting including the New Horizons Forum and Aerospace Exposition
4 - 7 January 2011, Orlando, Florida

AIAA 2011-1244

On Aerodynamic Design Through Multipoint Numerical Optimization

Howard P. Buckley, * and David W. Zingg †
Institute for Aerospace Studies, University of Toronto
4925 Dufferin St., Toronto, Ontario, M3H 5T6, Canada

A multipoint optimization approach is used to solve aerodynamic design problems encompassing a broad range of operating conditions. On-design and off-design operating conditions are represented as design points with corresponding objective and constraint functions. The use of a weighted integral as an objective function is demonstrated to improve aerodynamic performance over a range of on-design cruise conditions and also allows the designer to prioritize operating conditions based on mission requirements. Pareto fronts are presented as a useful tool in a multipoint design methodology enabling an understanding of trade-offs between competing design objectives which can aid the designer in improving the formulation of the design problem.

I. Introduction

The motivation behind this work is to develop an aerodynamic shape optimization framework that is capable of handling a comprehensive set of aerodynamic design requirements that must be given consideration when designing an aircraft. Given that an aircraft is subject to a widely varying set of operating conditions during a mission, it is desirable to design the aircraft such that it performs reasonably well over a range of flight-envelope conditions. In addition to optimizing performance at operating conditions defined by the mission specifications, constraints may be imposed to ensure that regulatory requirements associated with safety are satisfied. This is a general description of a practical aerodynamic design problem. In our multipoint optimization problem formulation, *on-design* points refer to the operating conditions where we wish to optimize aerodynamic performance according to specified design objectives. *Off-design* points refer to operating conditions that can be considered aerodynamic constraints to the optimization. For example, the off-design safety requirement that an aerodynamic shape must be able to achieve a specified maximum lift coefficient at low speeds constrains the potential for drag minimization at cruise conditions. Note that the off-design requirements are typically inequality constraints, and there is no benefit to surpassing the specifications.

Significant contributions to the area of multipoint optimization have been made by various researchers addressing practical design applications in 2D and 3D.[2,4,9,13] Multipoint optimization has been applied to tackle problems concerned with design for uncertainty and robustness[6,7] where the design objective is to desensitize aerodynamic performance to variation about some expected operating condition. Point optimization is often mentioned in discussions regarding multipoint design approaches. It refers to designs that exhibit rapid degradation in performance as one moves away from operating conditions specified at a design point. It is closely related to the concepts of robust design and design for uncertainty. Drela's hypothesis[3] states that point optimization will be encountered anytime the number of design variables exceeds the number of design points in an optimization. We find that point optimization is strongly related to the range of operating conditions and the distribution of design points over the range as shown by results presented in Section V.

Recently, a multipoint optimization method has been developed to solve practical aerodynamic design problems. A detailed description of the method can be found in Buckley et al.[1] along with preliminary

*Research Associate, howard@oddjob.utias.utoronto.ca
†Professor, Canada Research Chair in Computational Aerodynamics, J. Armand Bombardier Foundation Chair in Aerospace Flight, http://goldfinger.utias.utoronto.ca/ dwz

results showing that the method can be used to obtain an optimal solution to a practical aerodynamic design problem. The distinction between our method and others is in the scope of design considerations, which include not only on-design cruise conditions but also constraints at off-design conditions that are typically flow-dependent. In this paper, we revisit the design of a hypothetical aircraft utilizing our multipoint optimization method. We investigate the use of a new objective function which is formulated as a weighted integral of C_d over a range of on-design operating conditions. The danger of defining a multipoint objective function as the sum of drag coefficients at a discrete set of design points, as we have done previously, is that performance in between design points is not considered and may lead to instances of point optimization. The weighted integral approach is presented in Section V. It is applied to our original hypothetical aircraft test case as well as a new test case with a different set of on-design operating conditions to demonstrate its general use with suggestions for successful implementation.

To gain insight into the design space associated with the hypothetical aircraft test case, two sets of Pareto-optimal solutions are presented in Section VI providing a quantitative understanding of the trade-off between optimal on-design performance and satisfaction of off-design constraints and the trade-off between different on-design conditions. We wish to convey the idea that the knowledge of performance trade-offs obtained through optimization results gives the designer the opportunity to re-evaluate design priorities and clarify objectives. An appendix is included containing results from an investigation to determine guidelines for optimal grid density and number of design variables, with respect to computational efficiency, for solving a practical aerodynamic design problem.

The objective of this paper is to provide a methodology enabling the application of aerodynamic shape optimization to practical aerodynamic design.

II. Overview of Optima2D

Optima2D is a code for aerodynamic shape optimization developed by Nemec and Zingg[10, 11] that makes use of the following tools to solve practical aerodynamic design problems:

- Two-dimensional turbulent flow solver
- Airfoil geometry parametrization
- Discrete adjoint gradient calculation
- Mesh movement algorithm
- SQP constrained optimization algorithm

The compressible Reynolds-averaged Navier-Stokes equations are solved at each design iteration with a Newton-Krylov method in which the linear system arising at each Newton iteration is solved using the generalized minimal residual method (GMRES) preconditioned with an incomplete lower-upper (ILU) factorization with limited fill. Spatial derivatives in the governing equations are discretized using second-order centered finite differences with added scalar numerical dissipation. Eddy viscosity is computed using the one-equation Spalart-Allmaras turbulence model.

The airfoil geometry is parametrized using B-spline control points. The vertical coordinates of these control points are considered design variables, thus allowing alterations to the baseline shape. For lift-constrained drag minimization problems, the design variables are B-spline control points, and the angle of attack is computed as part of the flow solution in order to meet the lift constraint. For lift maximization problems, the angle of attack is a design variable in addition to the B-spline control points.

Gradients of objective and constraint functions that are dependent on the flow solution are calculated using the discrete-adjoint method; the adjoint equation is solved using preconditioned GMRES. Function and gradient evaluations are passed to the optimization algorithm, which determines how to modify the design variables in order to solve the optimization problem. At each design iteration, the grid around the updated airfoil shape is perturbed using a simple algebraic grid movement technique. The constrained optimization algorithm SNOPT developed by Gill, Murray, and Saunders[5] uses a sequential quadratic programming method that obtains search directions from a sequence of quadratic programming (QP) subproblems. Each QP subproblem minimizes a quadratic model of a Lagrangian function which is used to represent the objective function subject to linearized constraints.

III. Design Problem Definition

Operating Point	Reynolds Number	Mach Number	Lift Coefficient
A	27.32×10^6	0.72	0.17
B	27.32×10^6	0.72	0.28
C	18.57×10^6	0.72	0.27
D	18.57×10^6	0.72	0.45
E	24.22×10^6	0.64	0.21
F	24.22×10^6	0.64	0.36
G	16.46×10^6	0.64	0.34
H	16.46×10^6	0.64	0.57
I	28.88×10^6	0.76	0.28
J	28.88×10^6	0.76	0.15
K	28.88×10^6	0.76	0.46
L	28.88×10^6	0.76	0.25
M	19.62×10^6	0.76	0.45
N	19.62×10^6	0.76	0.24
O	19.62×10^6	0.76	0.74
P	19.62×10^6	0.76	0.40
Q	11.8×10^6	0.16	-
R	15.0×10^6	0.20	-

Table 1. Operating conditions for an 18-point optimization

The original test case considered by Buckley et al.[1] was based on a design specification for a hypothetical aircraft. The maximum weight of the aircraft is 100,000 lbs. Its wings are swept at 35 degrees and have an area of 1000 square feet. The aircraft maximum cruise speed is 0.88. Regions of the flight envelope considered for this design problem include cruise, long-range cruise, dive, and low-speed conditions. The design specification can be translated into a set of discrete design points that represent the above regions of the flight envelope. The flight envelope spans a range of values for Mach number, aircraft weight, and altitude. Table 1 summarizes 18 design points that are used to define this range of operating conditions. We use these design points as a basis for subsequent test cases investigated in this work.

The first four operating conditions, labeled A-D in Table 1, correspond to cruise. Due to the sweep angle, the effective Mach number is 0.72. Two sets of operating weights and altitudes are considered. For operating point A the altitude is 29,000 feet, the weight is 60,000 lbs.; for B the altitude is the same, but the weight is 100,000 lbs.; for C the altitude is 39,000 feet, the weight is 60,000 lbs.; for D the altitude is 39,000 feet, the weight is 100,000 lbs. The next four operating conditions, labeled E-H, correspond to long-range cruise. The Mach number is 0.78, producing an effective Mach number of 0.64. The altitudes and weights are the same as for A-D respectively.

The cruise and long-range cruise conditions represented by design points A-H are considered *on-design* operating conditions. This definition of on-design points is used in Pareto front test cases presented in Section VI where the objective function is defined as the sum of drag coefficients at these eight design points. In Section V a different set of on-design points is used to represent an approximation to the integral of C_d over the same range of operating conditions. The on-design performance goal for the cruise and long-range cruise conditions is to minimize drag over these regions of the flight envelope. We discuss the use of a weighting function in Section V to prioritize operating conditions based on the knowledge of the aircraft mission requirements.

The next eight operating conditions (I-P) are associated with a safety requirement for maneuverability under dive conditions. The flight Mach number is 0.93, making the effective Mach number 0.76. In addition to the two sets of weights and altitudes considered for the on-design points, two load factors are also taken into account. The combination produces a total of eight dive operating conditions. For operating point I, the altitude is 29,000 ft., the weight 60,000 lbs., and the load factor is 1.3. For operating point J, the altitude and weight are the same, but the load factor is 0.7. Operating points K and L have an altitude of 29,000 ft., a weight of 100,000 lbs., and load factors 1.3 and 0.7, respectively. For operating points M and N, the altitude is 39,000 ft., the weight is 60,000 lbs., and the load factors are 1.3 and 0.7, respectively. Operating points O and P have the same altitude and load factors, but the weight is 100,000 lbs. The dive

Operating Point	Operating Condition	On-Design Objective	Off-Design Constraint
A-D	cruise	lift-constrained drag minimization	-
E-H	long-range cruise	lift-constrained drag minimization	-
I-P	dive	-	$M_{max} \leq 1.35$
Q-R	low-speed	-	$C_{l,max} \geq 1.60$

Table 2. Design objectives and constraints for an 18-point optimization

maneuverability requirement is achieved by keeping shock strengths modest under these conditions, such that the Mach number upstream of a shock is less than or equal to 1.35.

The final two operating points reflect a safety requirement to be able to achieve an adequate maximum lift coefficient at low speed conditions. For operating condition Q, the altitude is sea level, the weight is 60,000 lbs., and the effective Mach number is 0.16. For operating point R the weight is 100,000 lbs., and the effective Mach number is 0.20. The safety requirement specifies that the maximum attainable lift coefficient under these conditions is at least 1.778.

The last ten design points, I-R, represent *off-design* operating conditions. The design requirements at these conditions impose constraints on the optimization. These eighteen operating points span the flight envelope. Table 2 summarizes the design objectives and constraints for this design problem. This design problem definition is meant to illustrate a basic set of on-design and off-design specifications that can be used to formulate a multipoint optimization problem. In practice, additional operating conditions, such as climb, also need to be considered, but can be easily accommodated by the methods referenced in this paper.

IV. Multipoint Optimization Problem Setup

This description of optimization setup parameters applies to the cases presented in subsequent sections. Unless otherwise specified, the airfoil geometry is parametrized using 15 B-spline control points. One control point is frozen at the leading edge and two at the trailing edge. The remaining 12 control points are designated as design variables and are split evenly between the top and bottom airfoil surfaces. Thickness constraints of 1% chord and 0.2% chord are imposed at 95% chord and 99% chord respectively to prevent trailing edge crossover. The latter is typically inactive once convergence is achieved. An area constraint requires that the area of the optimal geometry must be at least the area of the initial geometry. In all cases, the RAE 2822 airfoil is used as the initial geometry. Unless otherwise specified, the base grid has a C topology with 289 nodes in the streamwise direction and 65 nodes in the normal direction; the off-wall spacing is 2×10^{-6} chord. It was created using the RAE 2822 airfoil geometry. See the appendix for details on how the number of design variables and grid size was determined.

Off-design points I-P representing dive conditions are subject to the constraint that the maximum Mach number in the flow field not exceed 1.35. The maximum Mach number function used to represent this constraint is not continuous with respect to the design variables and therefore cannot be handled directly by SNOPT. To address this issue we use the Kreisselmeier-Steinhauser (KS) function[8] as a means to aggregate Mach number constraints evaluated at all nodes in the flow field into a single composite function that is continuously differentiable. M_{ks} represents a conservative estimate of the maximum Mach number in the flow field based on the KS function. Therefore, M_{max} constraints defined as $M^*_{max} - M_{max} \geq 0$, where the upper bound on the constraint is $M^*_{max} = 1.35$ translate to $M^*_{ks} - M_{ks} \geq 0$, where the upper bound on the constraint is $M^*_{ks} = 1.50$. This value of M^*_{ks} produces $M_{max} \leq 1.35$ at the optimal solution. An explanation of the determination of M^*_{ks} is provided in the appendix. Off-design points Q and R represent constraints at low-speed operating conditions such that $C_{l,max} - C^*_{l,max} \geq 0$, where the lower bound on the constraint is $C^*_{l,max} = 1.60$[a].

The flow solver described in Section II is used to evaluate airfoil performance in all cases. Given studies of the flow solver's accuracy performed by Zingg et al.,[12,14] the grids used can be expected to predict lift coefficients accurate to within 1% and drag coefficients to within 5% for attached and mildly separated flows,

[a]The optimization procedures applied to this design problem are demonstrated on a mesh of moderate density. Prior experience has shown that using a lower target lift coefficient of 1.60 on this mesh will yield a lift coefficient of at least 1.778 on a fine mesh used for accurate performance evaluation. See the appendix for further explanation of the off-design constraint values used with moderate grid densities suitable for optimization problems.

including both numerical and physical model error.

V. An Objective Function Defined as a Weighted Integral

Given the design objective of reducing drag over a range of cruise operating conditions, an objective function may be defined as the integral of C_d over the range of interest. Huyse and Lewis[6] propose a weighted integral approach for the purpose of solving robust optimization problems where the design objective is to desensitize aerodynamic performance of a shape to variability about some expected operating condition. In their approach to robust optimization, a weighting function represents the statistical variance of the prescribed operating condition. We apply the concept of a weighted integral to practical aerodynamic design problems in which a range of operating conditions are considered and a weighting function is utilized that allows the designer to prioritize the importance of operating conditions, e.g. based on mission requirements of the aircraft. The weighted integral is defined as

$$\int_{C_{l1}}^{C_{l2}} \int_{M_1}^{M_2} C_d\left(M, C_l\right) \mathcal{D}\left(M, C_l\right) dM dC_l \tag{1}$$

where $\mathcal{D}$ is a weighting function based on the priorities of the designer. Test cases presented in this section employ an arbitrarily defined designer-priority weighting function and are compared with cases where no designer priority is given to any of the operating conditions, i.e. $\mathcal{D} = 1$. The designer-priority weighting function used is given by

$$\mathcal{D}(M) = e^{a(M-M_1)} \tag{2}$$

$$a = \frac{\ln\left(10\right)}{M_2 - M_1} \tag{3}$$

The function $\mathcal{D}$ is defined such that at the endpoints of the Mach range, M_1 and M_2, $\mathcal{D}\left(M_1\right) = 1$ and $\mathcal{D}\left(M_2\right) = 10$ for $M_1 < M_2$. This particular function places ten times more importance on the high end of the Mach range than the low end. In terms of our hypothetical aircraft it could reflect the intention to fly most missions at cruise conditions A-D with the occasional mission flow at long-range cruise conditions E-H specified in Table 1.

The objective function to be minimized is an approximation of the weighted integral and is given by

$$\mathcal{J} = \sum_{i=1}^{N_M} \sum_{j=1}^{N_{Cl}} \omega_{i,j} C_d\left(M_i, C_{l_j}\right) \simeq \int_{C_{l1}}^{C_{l2}} \int_{M_1}^{M_2} C_d\left(M, C_l\right) \mathcal{D}\left(M, C_l\right) dM dC_l \tag{4}$$

where $N_M \times N_{Cl}$ is the number of design points used to discretize the range of operating conditions in M and C_l respectively. The design point weights, $\omega_{i,j}$, are given by

$$\omega_{i,j} = \mathcal{T}_{i,j} \mathcal{D}\left(M_i, C_{l_j}\right) \tag{5}$$

where $\mathcal{T}_{i,j}$ are the weights used to approximate the integral using the trapezoidal quadrature rule.

The accuracy of the integral approximation is dependent on the number of design points used in its evaluation and their distribution over the range of operating conditions. But how does accuracy of the integral approximation, which is used as the objective function, affect the optimal solution? And is the same level of accuracy required for design problems with different operating conditions? To answer these questions, the weighted integral approach is applied to several test cases described below.

A. Hypothetical Aircraft Test Case

The first case is the hypothetical aircraft design problem described in Section III. In this case, on-design operating conditions are represented by a four-point integral approximation. No designer-priority weighting function is used. The design points are located at the limits of the Mach number and C_l range. The Mach range is from 0.64 to 0.72. The range of lift coefficients is from 0.17 to 0.57. Off-design constraints I-R described in Section III as well as geometric constraints described in Section IV are imposed on the optimization. Figure 1 shows how C_d varies over the range of on-design operating conditions. The plots of

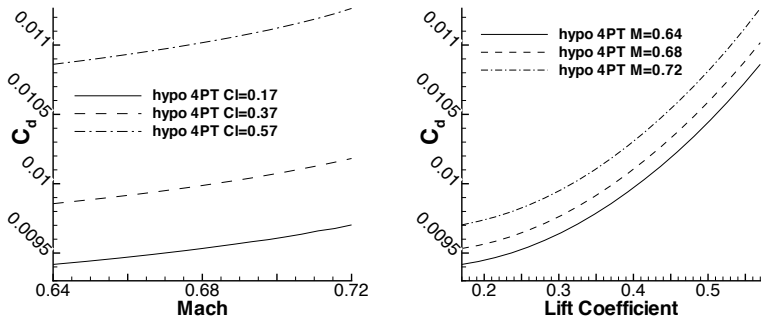

(a) C_d vs. Mach (b) C_d vs. C_l

Figure 1. C_d performance over the range of operating conditions for the optimal solution to the hypothetical aircraft test case obtained using a 4 point integral approximation

C_d versus Mach number and C_d versus C_l show that the drag performance is well behaved over the range of operating conditions. C_d increases monotonically with Mach number and C_l, and there is no evidence of point optimization. In this case, a four point integral approximation is an adequate representation of the exact integral. The error between the exact[b] integral and the approximate integral evaluated at the optimal solution is $\sim 2\%$. A four point integral approximation is adequate for this case because the function of C_d over the range of operating conditions exhibits near-linear behavoir. This seems to indicate that performance improvements at the design points are beneficial over the entire range of operating conditions. It is noteworthy that no point optimization is seen and the design is robust with respect to both Mach number and C_l.

B. Test Cases with Operating Conditions in the Drag Divergence Regime

In this section, we consider a different set of on-design operating conditions where it will be shown that a four-point integral approximation is insufficient. The range of cruise Mach numbers varies from 0.72 to 0.76. Lift requirements vary from $C_l = 0.64$ to $C_l = 0.74$. As with the hypothetical aircraft test case, these test cases are subject to off-design constraints I-R described in Section III as well as geometric constraints described in Section IV.

Two sets of optimizations are performed using integral approximations calculated with 4, 9, and 25 design points evenly distributed over the prescribed range of Mach numbers and lift coefficients. For the first set of optimizations, equal priority is given to all operating conditions, i.e. $\mathcal{D} = 1$, whereas the second set uses the exponential weighting function given by Equation 2.

Tables 3 and 4 show comparisons of the exact and approximate integrals evaluated at optimal solutions obtained using 4, 9, and 25 point integral approximations and the exact and approximate integrals evaluated using the initial geometry for cases using equal weighting and exponential weighting respectively. Both sets of results indicate that $\sim 2\%$ improvement in the exact integral is achieved when comparing the optimal solutions obtained with the four point integral approximations to solutions obtained with 25 point integral approximations. Examination of the values of C_d over the range of operating conditions reveals that significant differences in performance exist between optimal solutions obtained with approximate integral objective functions of varying accuracy. Figures 2 and 3 give a representative picture of how C_d performance varies over the range of operating conditions with the number of design points used in the integral approximation for both sets of optimal solutions. For both the exponential and the equal weighting cases it is clear that the four-point integral approximation is not an adequate representation of the C_d performance over the range of operating conditions given the significant point optimization observed in the vicinity of Mach 0.76. For the cases with equal weighting a significant difference in C_d performance is observed between the optimal solutions obtained with 4 and 9 point integral approximations compared to the negligible difference in performance between the optimal solutions obtained with 9 and 25 point integral approximations. In contrast to

[b]The exact integral is actually a very accurate approximation of the integral calculated using 361 sample points evenly spaced over the range of operating conditions.

Airfoil Geometry	Exact Integral $\left(\times 10^{-4}\right)$	Approx. Integral $\left(\times 10^{-4}\right)$	Error (%)
RAE 2822	0.7355	-	-
eqWt 4 PT	0.5253	0.5321	1.29
eqWt 9 PT	0.5155	0.5242	1.69
eqWt 25 PT	0.5149	0.5177	0.54

Table 3. Comparison of integral evaluations for RAE 2822 geometry versus optimal geometries obtained with 4, 9, and 25 point integral approximations and uniform weighting wrt to operating conditions

Airfoil Geometry	Exact Integral $\left(\times 10^{-3}\right)$	Approx. Integral $\left(\times 10^{-4}\right)$	Error (%)
RAE 2822	0.3338	-	-
exp 4 PT	0.2073	0.2972	43.38
exp 9 PT	0.2050	0.2293	11.85
exp 25 PT	0.2038	0.2105	3.29

Table 4. Comparison of integral evaluations for RAE 2822 geometry versus optimal geometries obtained with 4, 9, and 25 point integral approximations and exponential weighting wrt to operating conditions

these results are the optimal solutions for the cases using the exponential weighting function where it is clear that significant performance differences exist between all three levels of integral approximation accuracy. It seems logical that the amount of error in the approximate integral could be used as a criterion to determine the number of design points needed in its calculation. However, low-error integral approximations do not guarantee a desirable optimal solution as illustrated by the equal weighting solution obtained with a 4 point integral approximation. In this case, the error in the approximate integral is relatively low at 1.29% yet the solution exhibits point optimization.

The choice of designer-priority weighting function $\mathcal{D}$ has a dramatic impact on the performance of the optimal solution. A comparison of C_d performance between the optimal solutions for the equal and exponential weighting cases with 25 point integral approximations is shown in Figure 4. Figure 5 shows the average drag coefficient over the range of lift coefficients as a function of Mach number, where each data point represents the integral of C_d over the range of C_l divided by ΔC_l. Both solutions are robust with respect to Mach number and C_l. The exponential weighting function produces significantly better performance at the high-end Mach numbers, where an improvement in C_d of greater than 10% is achieved compared to the result obtained with equal weighting. The cost of better performance at high Mach numbers is inferior performance over the low to mid-range Mach numbers compared to the equal weighting result. As the tradeoffs between the two solutions are clearly shown, the designer has the opportunity re-evaluate design priorities and fine-tune the weighing function $\mathcal{D}$ if desired.

We have used the weighted integral approach to obtain optimal solutions to three unique design problems. Given the differences in performance for each case, it is not surprising that there are significant differences in optimal airfoil geometries for these cases. Figure 6 compares optimal airfoil geometries obtained for the exponential and equal weighting cases with 25 point integral approximations as well as the hypothetical aircraft test case with a 4 point integral approximation.

These results show that an appropriate quadrature for calculating the approximate integral objective function is necessary to achieve an optimal and robust solution. The approximate integral must adequately model the complexity of the $C_d\mathcal{D}$ (designer-weighted drag) function. Otherwise the optimal solution minimizes a poor representation of the function. This may produce a design with undesirable performance such as the significant point optimization exhibited in these cases. An appropriate quadrature for a given design problem depends on several factors, including the weighting function used to prioritize the operating conditions and the range of operating conditions considered.

VI. Pareto Fronts

Design via aerodynamic shape optimization can be considered an iterative process. The optimization process is capable of more than just producing the optimal shape. It can also provide the designer with information on various trade-offs which can be used to reformulate the objectives and constraints. The

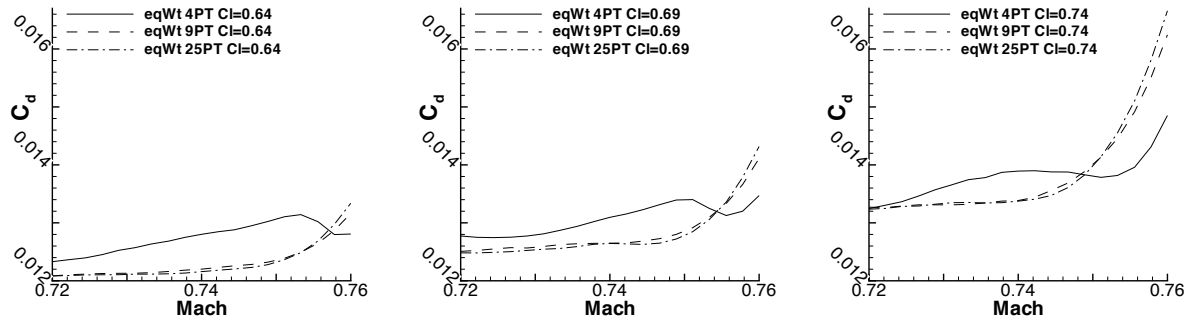

(a) $C_l = 0.64$ (b) $C_l = 0.69$ (c) $C_l = 0.74$

Figure 2. C_d versus Mach for optimal solutions obtained with 4, 9, and 25 point integral approximations and equal weighting wrt operating conditions

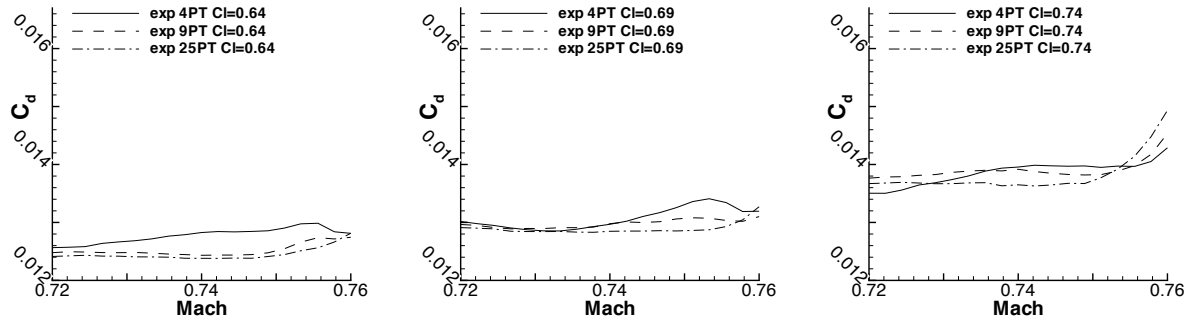

(a) $C_l = 0.64$ (b) $C_l = 0.69$ (c) $C_l = 0.74$

Figure 3. C_d versus Mach for optimal solutions obtained with 4, 9, and 25 point integral approximations and exponential weighting wrt operating conditions

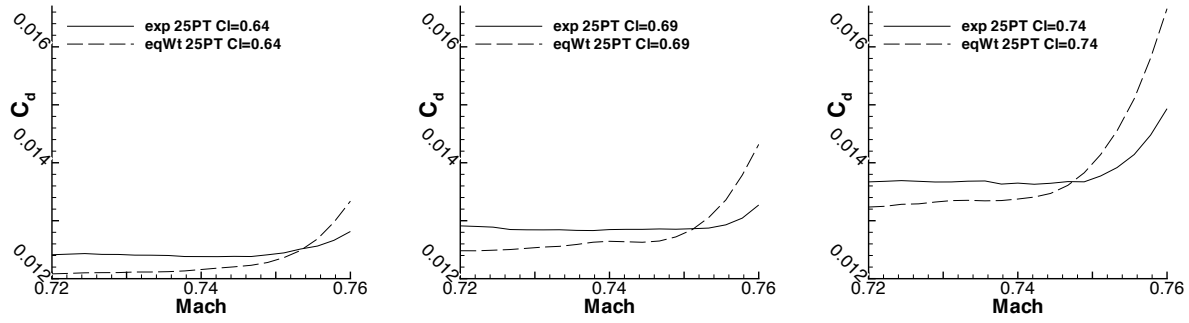

(a) $C_l = 0.64$ (b) $C_l = 0.69$ (c) $C_l = 0.74$

Figure 4. A comparison of C_d performance over the range of operating conditions between optimal solutions for exponential and equal weighting cases with 25 point integral approximations

problem specification may evolve over several iterations until the final solution is a suitable compromise between all design objectives and constraints. As shown in Section V, experimenting with different weighting functions not only allows the designer to tailor the solution to suit mission requirements but also provides knowledge of performance trade-offs associated with prioritizing on-design operating conditions. Similarly,

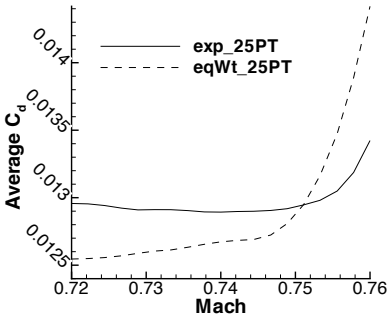

Figure 5. Comparison of the average drag coefficient over the range of lift coefficients versus Mach number between optimal solutions for exponential and equal weighting cases with 25 point integral approximations

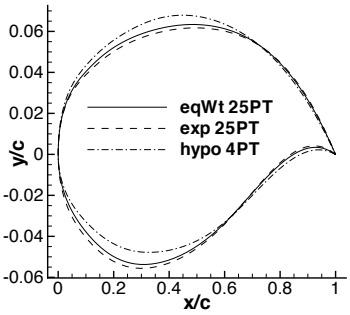

Figure 6. Comparison of optimal airfoil geometries for exponential and equal weighting cases with 25 point integral approximations as well as the hypothetical aircraft test case with a 4 point integral approximation

Pareto fronts can be used to probe the design space to yield information on any pair of competing objectives that are of interest.

A. Cruise Versus Long-Range Cruise

As described in Section III, the on-design operating conditions are divided into cruise conditions (Points A-D) and long-range cruise conditions (Points E-F) [c]. The main design objective over all cruise conditions is to minimize an unweighted sum of the eight drag coefficients. However, a designer may be curious to know the price paid in terms of C_d at cruise conditions to have a shape that also performs well at long-range cruise conditions and vice versa. A Pareto front was generated to answer this question. For this Pareto front study, two design objectives are considered; to minimize the sum of C_d at cruise conditions A-D, and to minimize the sum of C_d at long-range cruise conditions E-F. A set of optimal solutions is obtained by minimizing the weighted objective function given by

$$\mathcal{J} = \omega \sum_{p=1}^{\substack{\#\text{ of}\\ \text{cruise pts}}} \mathcal{J}_p^{\text{cruise}} + (1-\omega) \sum_{q=1}^{\substack{\#\text{ of}\\ \text{LR cruise pts}}} \mathcal{J}_q^{\text{LR-cruise}} \tag{6}$$

at values of $\omega \in [0,1]$ where $\mathcal{J}^{\text{cruise}}$ and $\mathcal{J}^{\text{LR-cruise}}$ represent values of C_d at cruise and long-range cruise conditions. Figure 7 shows the resulting Pareto front. It is apparent from this figure that the cruise and long-range cruise design objectives are quite insensitive to one another, given that favouring one objective over the other results in a change in C_d of less than 0.2%. This demonstrates that there is not much competition between these two sets of design objectives. Given these results, the designer now understands

[c]This is the same range of on-design conditions considered in the test case described in Section V-A. However, the objective function in that case is defined as a 4 point approximation to the integral of C_d over the range of operating conditions.

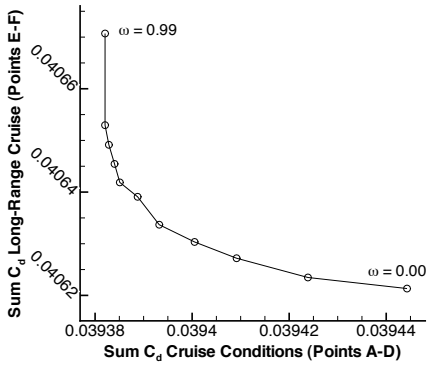

Figure 7. Cruise versus long-range cruise Pareto front

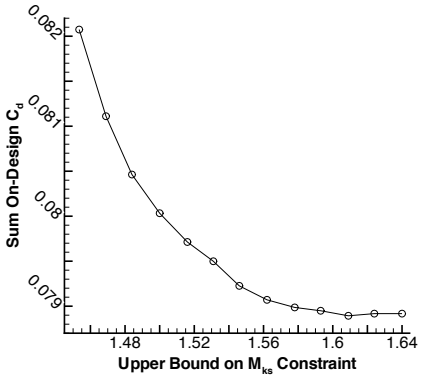

Figure 8. Sum of on-design C_d's versus M_{ks} constraint Pareto front

that specifying long-range cruise conditions in the optimization problem is somewhat redundant and may be excluded with little consequence. Alternatively, based on this information, the designer may choose to increase the cruise speed knowing that the impact on long-range cruise performance will not be excessive.

B. On-Design Performance Versus M_{ks} Constraint

A designer may also be interested in the sensitivity of on-design performance to off-design constraints. The off-design constraint associated with dive conditions shown in Table 2 is $M_{max} \leq 1.35$. Setting the upper bound on $M_{ks} = 1.50$ will achieve satisfaction of this constraint at all dive operating conditions[d]. The Pareto front shown in Figure 8 consists of a set of optimal solutions generated by incrementally relaxing the upper bound on the M_{ks} constraint from 1.46 to 1.64. At the right end of the front it can be seen that increasing M_{ks} beyond 1.61 does not improve on-design performance. This point coincides with the value of M_{ks} at which the constraint becomes inactive. The corresponding M_{max} value is 1.44 which remains constant for $M_{ks} \geq 1.61$. Moving from right to left along the front shows on-design performance becomes increasingly penalized as the constraint upper bound becomes more restrictive. In this case, if the designer has the freedom to relax the constraint from $M_{ks} = 1.50$, a performance improvement of up to 2% may be realized. This is important information to the designer if there exists an alternative means of achieving the safety requirement addressed by the constraint.

[d] M_{ks} is described in Section IV and the appendix

VII. Conclusions

Optimizations performed using an objective function based on a weighted integral demonstrate an effective technique for improving performance over a range of operating conditions. Given a sufficiently accurate quadrature, the weighted integral approach enables the computation of an optimal and robust design. The weighted integral approach also affords the designer a formal way of prioritizing a range of operating conditions based on mission requirements. The accuracy of the approximation of the weighted integral is dependent on the number of design points used and their distribution over the range of operating conditions as well as the degree of non-linearity of the C_d function over the range of operating conditions. Examples of Pareto fronts are given that provide the designer with helpful information that can be used in defining the optimization problem. Based on this information about various trade-offs of interest, the designer can reformulate the objective and constraints as the optimization progresses.

Acknowledgements

The funding of the first author by the Natural Sciences and Engineering Research Council of Canada and the second author by the Natural Sciences and Engineering Research Council of Canada and the Canada Research Chairs program is gratefully acknowledged.

Computations were performed on the GPC supercomputer at the SciNet HPC Consortium. SciNet is funded by: the Canada Foundation for Innovation under the auspices of Compute Canada; the Government of Ontario; Ontario Research Fund - Research Excellence; and the University of Toronto.

References

[1]H. Buckley, B. Zhou, and D. W. Zingg. Airfoil Optimization Using Practical Aerodynamic Design Requirements. *Journal of Aircraft*, 47(5):1707–1719, September-October 2010.

[2]S. E. Cliff, J. J. Reuther, D. A. Saunders, and R. M. Hicks. Single-Point and Multipoint Aerodynamic Shape Optimization of High Speed Civil Transport. *Journal of Aircraft*, 38(6):997–1005, 2001.

[3]M. Drela. *Frontiers of Computational Fluid Dynamics*, chapter Pros and Cons of Airfoil Optimization, pages 363–381. World Scientific, 1998.

[4]B. Epstein, A. Jameson, S. Peigin, D. Roman, N. Harrison, and J. Vassberg. Comparative Study of Three-Dimensional Wing Drag Minimization by Different Optimization Techniques. *Journal of Aircraft*, 46(2):526–541, March-April 2009.

[5]P. E. Gill, W. Murray, and M. A. Saunders. SNOPT: An SQP Algorithm for Large-Scale Constrained Optimization. *SIAM Review*, 47(1):99–131, February 2005.

[6]L. Huyse and R. M. Lewis. Aerodynamic Shape Optimization of Two-Dimensional Airfoilis Under Uncertain Operating Conditions. TM CR-2001-210648, NASA, 2001.

[7]L. Huyse, S. L. Padula, R. M. Lewis, and W. Li. Probabilistic Approach to Free-Form Airfoil Shape Optimization Under Uncertainty. *AIAA Journal*, 40(9), September 2002.

[8]G. Kreisselmeier and R. Steinhauser. Systematic Control Design by Optimizing a Vector Performance Index. In *International Federation of Active Controls Symposium on Computer-Aided Design of Control Systems*, Zurich, Switzerland, August 29-31 1979.

[9]W. Li, L. Huyse, and S. Padula. Robust Airfoil Optimization to Achieve Consistent Drag Reduction Over a Mach Range. *Structural and Multidisciplinary Optimization*, 24(1):38–50, 2002.

[10]M. Nemec and D. W. Zingg. Newton-Krylov Algorithm for Aerodynamic Design Using the Navier-Stokes Equations. *AIAA Journal*, 40(6):1146–1154, June 2002.

[11]M. Nemec, D. W. Zingg, and T. H. Pulliam. Multipoint and Multi-Objective Aerodynamic Shape Optimization. *AIAA Journal*, 42(6):1057–1065, June 2004.

[12]D. W. Zingg. Grid Studies for Thin-Layer-Navier-Stokes Computations of Airfoil Flowfields. *AIAA Journal*, 30(10):2561–2564, 1992.

[13]D. W. Zingg and S. Elias. Aerodynamic Optimization Under a Range of Operating Conditions. *AIAA Journal*, 44(11):2787–2792, November 2006.

[14]D. W. Zingg, S. De Rango, M. Nemec, and T. H. Pulliam. Comparison of Several Spatial Discretizations for the Navier-Stokes Equations. *Journal of Computational Physics*, 160(2):683–704, May 2000.

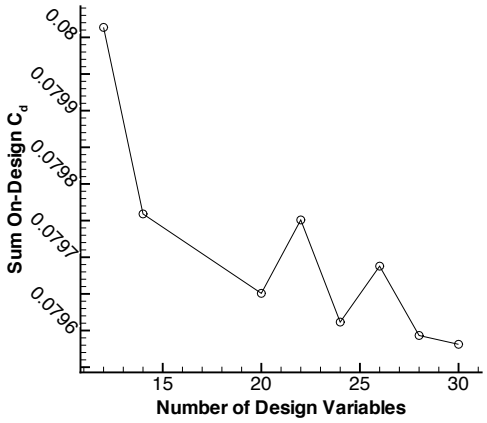

Figure 9. Sum of on-design C_d's versus number of design variables

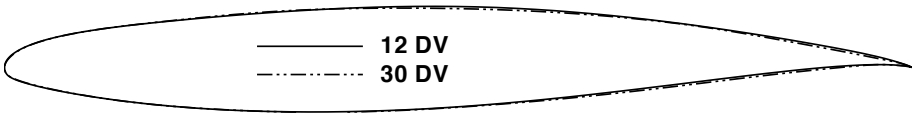

Figure 10. Comparison of optimized airfoil geometries with 12 and 30 design variables

A. Optimal Parameters For Practical Aerodynamic Design Problems

A preliminary study of the design problem described in Section III used an airfoil geometry parametrized by 15 B-spline control points, 12 of which were used as geometric design variables, and a grid size of 18785 nodes. These values have been revisited to study their effect on the optimal solution to the design problem. Given that computational effort increases with grid size and number of design variables, a study of these parameters aims to determine values that minimize computational effort while attaining a satisfactory solution to the design problem.

A. Design Variable Study

Optimizations were performed with number of design variables ranging from 12 to 30. Figure 9 shows a slight trend toward on-design performance improvement as the number of design variables are increased. The difference between the best and worst on-design performance, at 30 design variables and 12 design variables respectively, is approximately 0.6%. A comparison of the optimized airfoil geometries obtained with 30 design variables and 12 design variables is shown in Figure 10. The main differences in airfoil geometry are observed at the trailing edge as shown in Figure 11. The trailing edge at 30 design variables presents manufacturing and structural difficulties because it is extremely thin. The additional design variables create a requirement for some additional thickness constraints, which will reduce the already small benefit of increasing the number of design variables. Table 5 shows the number of function evaluations (where a function evaluation requires one computation of a flow solution) required as the number of design variables increases. It can be seen that the computational effort increases significantly with the number of design variables. When weighing the benefit of modest performance improvements achieved with greater number of design variables against increased computational effort and infeasible airfoil geometry with respect to manufacturing and structural concerns, using 12-14 design variables is recommended, as values in this range provide a sufficiently optimal solution to this design problem and will likely be suitable for design problems with similar operating conditions.

Number of Design Variables	Number of Function Evaluations
12	47
14	41
20	141
22	133
24	134
26	152
28	164
30	232

Table 5. Number of function evaluations versus number of design variables

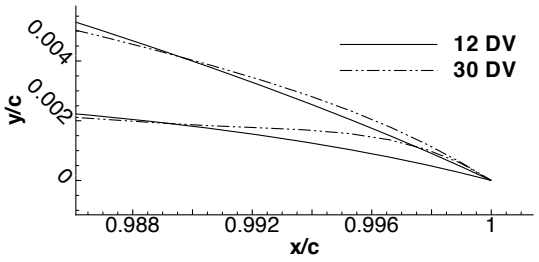

Figure 11. Comparison of optimized airfoil trailing edges with 12 and 30 design variables

B. Grid Density Study

To investigate the effect of grid size on the optimal solution, optimizations are performed using the coarse and fine grids described in Table 6. Performance of the optimal solution at each grid size is evaluated using the evaluation grid, which is extremely fine and produces very accurate lift and drag coefficients. The hypothetical aircraft design problem described in Section III is used as the test case.

An iterative optimization procedure is required to ensure that active off-design constraints are comparably satisfied at optimal solutions for each grid size when evaluated on the evaluation grid. This is because the values of the constraint bounds at each grid that will satisfy the constraints when evaluated on the evaluation grid are not known beforehand. The design problem described in Section III specifies that the maximum Mach number at dive conditions I - O must not exceed 1.35 and that $C_{l,max} \geq 1.778$ at high-lift conditions Q - R. It is known that our flow solver will under-predict these constraint values in proportion to the grid size. To address this issue, an initial guess for the constraints is used at each grid size. The initial guess is based on evaluation of the constraints at the initial geometry using both the coarse grid and the evaluation grid. A converged optimal solution is obtained using the initial guess for the constraint bounds. The constraints are evaluated using the optimal solution on the evaluation grid. The constraint bounds are updated according to the following formulas and used for the next optimization iteration:

$$\left(C^*_{l,max}\right)^{n+1}_{(C)} = \left(C^*_{l,max}\right)_{(E)} - \left[(C_{l,max})^n_{(E)} - (C_{l,max})^n_{(C)}\right] \tag{7}$$

$$(M^*_{max})^{n+1}_{(C)} = (M^*_{max})_{(E)} - \left[(M_{max})^n_{(E)} - (M_{max})^n_{(C)}\right] \tag{8}$$

Subscripts C and E denote constraint evaluations on coarse grids and the evaluation grid respectively and the superscript is the index of optimization iterations. $(C^*_{l,max})^n_{(C)}$ is the lower bound on the high lift constraint used on the coarse grid at optimization iteration n. $(C^*_{l,max})_{(E)}$ is the lower bound on the high lift constraint used on the evaluation grid. This is the constraint value we are trying to achieve, i.e. $C_{l,max} \geq 1.778$. $(C_{l,max})^n_{(E)}$ is the value of the high lift constraint evaluated on the evaluation grid at optimization iteration n. $(C_{l,max})^n_{(C)}$ is the value of the high lift constraint evaluated on the coarse grid at optimization iteration n. An analogus naming convention is used in the M_{max} constraint bound update formula.

After three optimization iterations the constraints for optimal solutions at each grid are satisfied to within a tolerance of ± 0.005 when evaluated on the evaluation grid. Table 7 shows a comparison of the sum of drag

Grid Name	Size	Off-wall Spacing (chord)
coarse	289×65	2.0×10^{-6}
fine	401×89	2.0×10^{-6}
evaluation	917×193	7.5×10^{-7}

Table 6. Grids used to study the effect of grid density on the optimal solution

Grid Name	Sum of On-Design C_d	$(Cl_{,max})_{(E)}$	$(C^*_{l,max})_{(C)}$	$(M_{max})_{(E)}$	$(M^*_{max})_{(C)}$
coarse	0.06632	1.778	1.5706	1.355	1.281
fine	0.06566	1.779	1.628	1.352	1.301

Table 7. Comparison of on-design performance and active off-design constraints computed on the evaluation grid for optimal solutions obtained with three different grid sizes

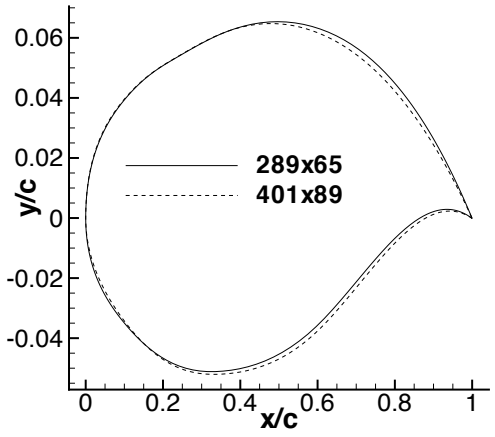

Figure 12. Comparison of optimal airfoil geometries obtained using different grid densities

coefficients at on-design operating conditions evaluated using the evaluation grid with the optimal solution at each grid size. A comparison of the active off-design constraints evaluated using the evaluation grid with the optimal solution at each grid size is also given in Table 7. Figure 12 shows a comparison of the optimal geometries at each grid size. A 1% performance improvement in the optimal solution has been achieved using the fine grid versus the coarse grid. A slight difference in the optimal geometries is visible.

C. Determination of Maximum Mach Number Constraint Bound M^*_{ks}

As described by Buckley et. al[1] and reviewed in Section IV, the KS function provides a conservative estimate of the maximum Mach number in the flow field that is used as the basis for the maximum Mach number constraint associated with dive conditions. At dive conditions, $M_{max} \leq M^*_{max}$. M^*_{ks} is defined as the bound on the conservative estimate of maximum Mach number based on the KS function. M^*_{max} is the actual bound on maximum Mach number in the flow field. M_{max} is the maximum Mach number evaluated at the optimal solution. At an optimal solution, SNOPT ensures that M_{ks} at all dive conditions does not exceed M^*_{ks}. It is not known beforehand what value of M^*_{ks} will produce $M_{max} \leq M^*_{max}$. The iterative procedure described below is used to obtain the appropriate value of M^*_{ks} for a given design problem:

1. Start with an initial guess for M^*_{ks}: $M^*_{ks} = M^0_{ks}$
2. Run the optimization until a converged solution is obtained
3. Calculate the discrepancy in M_{max} : $\Delta M_{max} = M^*_{max} - M_{max}$
4. Update guess for M^*_{ks}: $M^*_{ks} = M^1_{ks} = M^0_{ks} + \Delta M_{max}$

5. Restart the optimization using updated value for M_{ks}^*

6. Repeat steps 2 - 5 until $M_{max} \simeq M_{max}^*$ at the converged solution to within some specified tolerance

The maximum Mach number constraint can be satisfied to within $\pm 1 \times 10^{-4}$ in 5 iterations.